

ON THE ABSENCE OF NON-THERMAL X-RAY EMISSION AROUND RUNAWAY O STARS

J.A. TOALÁ (杜宇君)¹, L.M. OSKINOVA², AND R. IGNACE³

¹Institute of Astronomy and Astrophysics, Academia Sinica (ASIAA), Taipei 10617, Taiwan

²Institute for Physics and Astronomy, University of Potsdam, D-14476 Potsdam, Germany

³Department of Physics and Astronomy, East Tennessee State University, Johnson City, TN 37614, USA

ABSTRACT

Theoretical models predict that the compressed interstellar medium around runaway O stars can produce high-energy non-thermal diffuse emission, in particular, non-thermal X-ray and γ -ray emission. So far, detection of non-thermal X-ray emission was claimed for only one runaway star AE Aur. We present a search for non-thermal diffuse X-ray emission from bow shocks using archived *XMM-Newton* observations for a clean sample of 6 well-determined runaway O stars. We find that none of these objects present diffuse X-ray emission associated to their bow shocks, similarly to previous X-ray studies toward ζ Oph and BD+43°3654. We carefully investigated multi-wavelength observations of AE Aur and could not confirm previous findings of non-thermal X-rays. We conclude that so far there is no clear evidence of non-thermal extended emission in bow shocks around runaway O stars.

Keywords: stars: massive — stars: mass-loss — stars: winds, outflows — X-rays: ISM — stars: individual (AE Aur, BD−14°5040, HD 24760, HD 57682, HD 153919, HD 188001, HD 210839)

1. INTRODUCTION

Massive ($M_i > 10 M_\odot$), runaway ($v_\star \gtrsim 30 \text{ km s}^{-1}$) stars are able to produce large-scale bow shocks in the Interstellar Medium (ISM). These shocks are driven by the interaction of the fast stellar wind ($v_\infty \gtrsim 1000 \text{ km s}^{-1}$), large proper motion, and the ISM. The gas and dust in the pile-up material are heated and ionized by the strong UV radiation from the star which makes the bow shock observable at optical and infrared (IR) wavelengths (e.g., Kaper et al. 1997; Peri et al. 2015, and references therein).

Benaglia et al. (2010) analyzed Very Large Array (VLA) observations of the runaway O star BD+43°3654 and concluded that the radio emission is spatially coincident with the bow shock detected in IR images. More importantly, this extended radio emission was found to have a non-thermal origin. Benaglia et al. argued that the non-thermal origin of the radio emission is produced by synchrotron emission. The electrons that generate this emission could upscatter photons from stellar and dust radiation fields through the inverse Compton process, producing high-energy emission. This interesting detection opened a new window for exploring the production of non-thermal emission around massive stars, and a number of theoretical works addressing this phenomenon have been published (e.g., del Valle et al. 2015, and references therein).

del Valle & Romero (2012) presented detailed analytical predictions for the non-thermal emission from bow shocks around O-type stars. These authors applied their model to the well-known and closest runaway star ζ Oph, concluding that high-energy emission should be detected toward its bow shock. However, X-ray and γ -ray emission has been eluding detection towards known runaway stars. Schulz et al. (2014) presented Fermi γ -ray Space Telescope observations of a sample of 27 bow shocks (including ζ Oph) accumulated over 57 months with no positive detections. Schulz et al. (2016) extended this study up to 73 bow shocks using the H.E.S.S. telescopes in the TeV regime with the same conclusions. In X-rays no detections were obtained either, despite the dedicated observational campaigns using *Chandra*, *XMM-Newton*, and *Suzaku* X-ray telescopes (Terada et al. 2012; Toalá et al. 2016).

There has been only one claim of detection of non-thermal X-ray emission toward a runaway star. López-Santiago et al. (2012) presented *XMM-Newton* observations of AE Aur and reported the discovery of a “blob” of X-ray emission at $\gtrsim 30''$ northeast from the star. These authors also presented a model to explain their results, but we notice that their spectral analysis cannot be used to discriminate between a thermal and a non-thermal origin. Furthermore, these authors compare their *XMM-Newton* observations with low-resolution mid-IR *WISE* observations. Under the assumption that this detection is related to AE Aur,

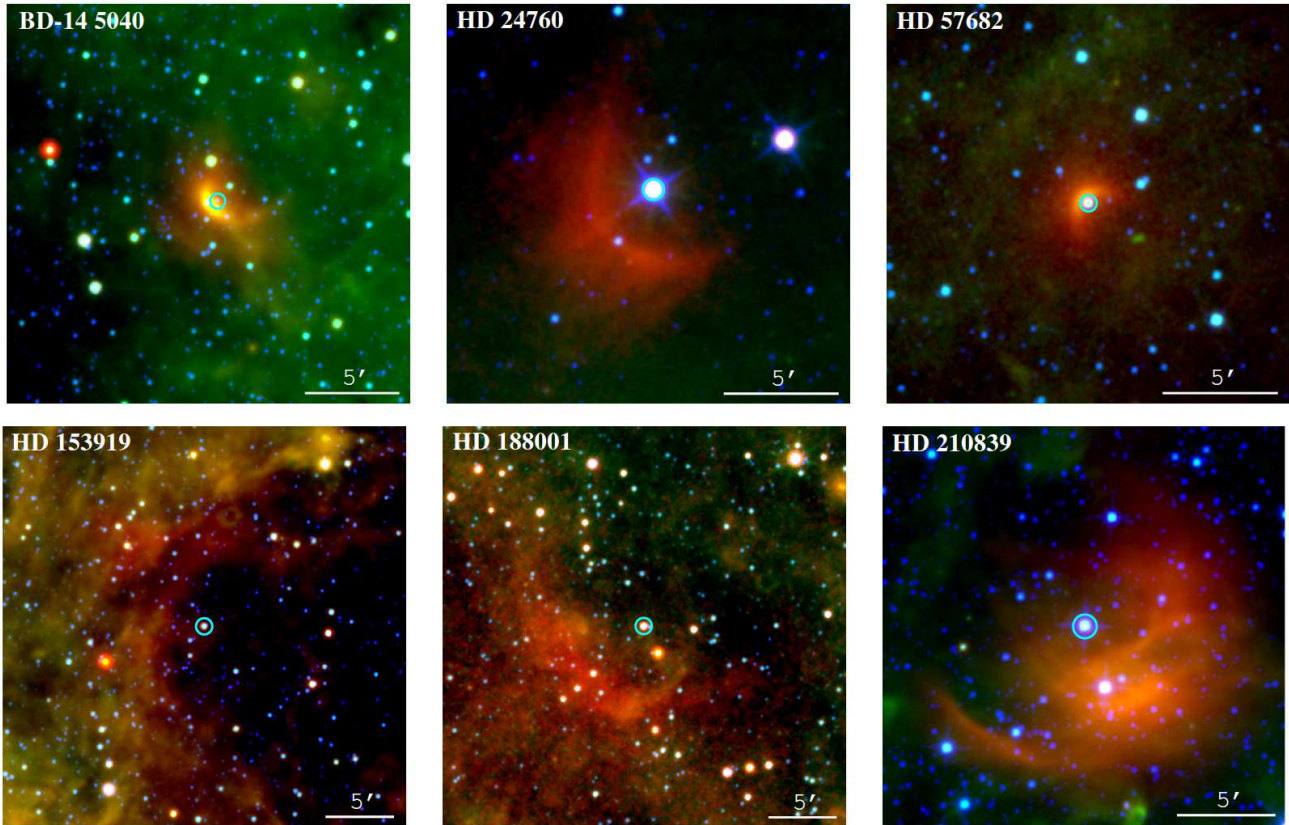


Figure 1. Composite colour mid-IR *WISE* images of the bow shocks around the O stars studied in this paper. Red, green, and blue correspond to the W4 ($22 \mu\text{m}$), W3 ($12 \mu\text{m}$), and W2 ($4.6 \mu\text{m}$) bands, respectively. A circular aperture on each panel shows the position of the stars. North is up, east to the left.

Pereira et al. (2016) presented further analytical modelling for this X-ray emission. They concluded that non-thermal processes in bow shocks around runaway stars are responsible for a significant fraction of the high-energy photons produced in our Galaxy.

In this paper we present a search for non-thermal diffuse X-ray emission in bow shocks around O-type stars. We use archived *XMM-Newton* observations of a sample of well-determined galactic runaway stars. Section 2 presents our sample and describe the *XMM-Newton* observations. In Section 3 and 4 we presents and discuss our results, respectively. Finally, we present our conclusions in Section 5.

2. OBSERVATIONS - THE SAMPLE

To obtain a clear sample of runaway O stars we searched the list presented by Maíz Apellániz et al. (2016). These authors identified runaway stars using the proper motions reported by the first Gaia Data Release (DR1; Brown et al. 2016). Their table 1 presents a list of confirmed candidates as well as a list of new discoveries. We cross-correlated that table with archived *XMM-Newton* EPIC observations and clear detections of bow shocks in the *WISE* W4 $22 \mu\text{m}$ or *Spitzer* MIPS $24 \mu\text{m}$

band. As a result, our sample consists of 6 objects: BD-14°5040, HD 24760 (ϵ Per), HD 57682, HD 153919, HD 188001 (9 Sge), and HD 210839 (λ Cep). Figure 1 presents mid-IR colour-composite *WISE* images of the six objects studied in this paper.

Details of the X-ray observations used in this paper are given in Table 1. Columns 5, 6, and 7 of Table 1 present the total exposure time for the pn, MOS1, and MOS2 EPIC cameras, respectively. It is worth mentioning that almost all observations were performed with deep exposures ($t_{\text{exp}} > 30$ ks), except for the cases of HD 24760 and HD 57682 ($t_{\text{exp}} \gtrsim 10$ ks). Observations of BD-14°5040 were only performed using the MOS cameras but with deep exposure times of $t_{\text{exp}} \sim 70$ ks. Finally, we remark that the EPIC cameras have a FWHM $\approx 6''$.

3. ANALYSIS AND RESULTS

The *XMM-Newton* EPIC observations were processed using the Science Analysis Software (SAS) version 15.0 and the calibration access layer available on 2017 January 6. All observation data files (ODF) were processed using the SAS tasks *epproc* and *emproc* to produce the event files. In order to identify and excise periods of

Table 1. Observation details

Object	R.A. (J2000)	Dec. (J2000)	Obs. ID.	Total exposure time			Net exposure time		
				pn (ks)	MOS1 (ks)	MOS2 (ks)	pn (ks)	MOS1 (ks)	MOS2 (ks)
BD−14°5040	18:25:38.90	−14:45:05.74	0742980101	—	72.62	72.63	—	69.52	69.55
HD 24760	03:57:51.23	40:00:36.78	0761090801	14.04	15.66	15.63	6.42	8.70	8.90
HD 57682	07:22:02.06	−08:58:45.77	0650320201	8.73	11.45	11.47	6.02	8.87	9.47
HD 153919	17:03:56.88	−37:50:38.91	0600950101	42.78	50.27	50.37	41.40	50.27	50.07
HD 188001	19:52:21.76	18:40:18.75	0743660201	26.76	31.34	31.32	26.76	31.34	31.32
HD 210839	22:11:30.57	59:24:52.15	0720090501	83.82	93.94	93.99	73.49	92.70	92.34

high background level, we created light curves of the background, binning the data over 100 s for each of the EPIC camera. The final net exposure times for each EPIC cameras are listed in columns 8, 9, and 10 in Table 1.

To unveil the presence of diffuse X-ray emission around the runaway stars studied here, we made use of the XMM-ESAS tasks which are optimized for the identification of extended sources, to produce images in different energy bands. These algorithms also help identify point-like sources projected in the line of sight of the bow shocks. For each object, we created exposure-map-corrected, background-subtracted EPIC images in three different energy bands, namely 0.3–1.0 (soft), 1.0–2.0 (medium), and 2.0–5.0 keV (hard), following the Snowden & Kuntz’s cookbook for analysis of *XMM-Newton* EPIC observations of extended objects and diffuse background (Snowden & Kuntz 2011). All images have been adaptively smoothed using the ESAS task *adapt* requesting 10 counts under the smoothing kernel of the original images. The resultant images for each target are presented in Figure 2.

Figure 2 shows that all progenitor stars are detected in X-rays as well as a large number of point sources in the field of view of the observations. Furthermore, Fig. 2 clearly shows the absence of diffuse X-ray emission in the six bow shocks around our targets. To highlight the absence of detected X-ray emission from bow shocks, all panels of Fig. 2 also present contours corresponding to the mid-IR emission as detected by the *WISE* W4 22 μm band, where the extended X-ray emission was expected.

4. DISCUSSION

The detection of non-thermal radio emission associated with the bow shock around BD+43°3654 (Benaglia et al. 2010) opened a door for studies of particle acceleration by massive stars. Those VLA observations showed that the non-thermal emission has an extended distribution, spatially coincident with the bow shock observed by the Midcourse Space Experiment

Table 2. Estimated X-ray fluxes

Object	N_{H}	f_{X}	F_{X}
	$\times 10^{21} \text{ cm}^{-2}$	$\text{erg cm}^{-2} \text{ s}^{-1}$	$\text{erg cm}^{-2} \text{ s}^{-1}$
BD−14°5040	10.7	3.3×10^{-15}	6.4×10^{-15}
HD 24760	2.8	1.0×10^{-14}	1.4×10^{-14}
HD 57682	4.4	4.2×10^{-15}	6.6×10^{-15}
HD 153919	7.2	7.0×10^{-15}	1.2×10^{-14}
HD 188001	2.8	1.7×10^{-16}	2.5×10^{-16}
HD 210839	9.2	7.4×10^{-15}	1.4×10^{-14}

(MSX) in the D (14.65 μm) band¹. Since then, the idea that charged particles in the compress ISM (the bow shock) can cool down by non-thermal processes (such as synchrotron radiation), has been studied extensively in theoretical studies (see Pereira et al. 2016, and references therein). But the absence of firmly confirmed detections of high-energy non-thermal emission is pushing the limits of theory, even for the case of BD+43°3654.

In order to estimate upper limits to the non-thermal diffuse X-ray emission, we extracted background-subtracted spectra from regions spatially coincident with the bow shocks in our sample. The obtained background count rates in the 0.3–5.0 keV energy range along with the estimated hydrogen column densities (N_{H})² were used to obtain absorbed (f_{X}) and unabsorbed (F_{X}) X-ray fluxes. Using the *Chandra* PIMMS tool³ we estimated the fluxes assuming that the emission can be modeled by a power-law spectrum with $\Gamma = 1.5$. Table 2

¹ We note that fig. 3 in Benaglia et al. (2010) shows a clump with positive spectral index which is not associated with the bow shock, in fact this feature is a clump easily spotted in the *WISE* W3 12 μm image presented by Toalá et al. (2016).

² We used the *Chandra* Galactic Neutral Hydrogen Density Calculator: <http://cxc.harvard.edu/toolkit/colden.jsp>

³ <http://cxc.harvard.edu/toolkit/pimms.jsp>

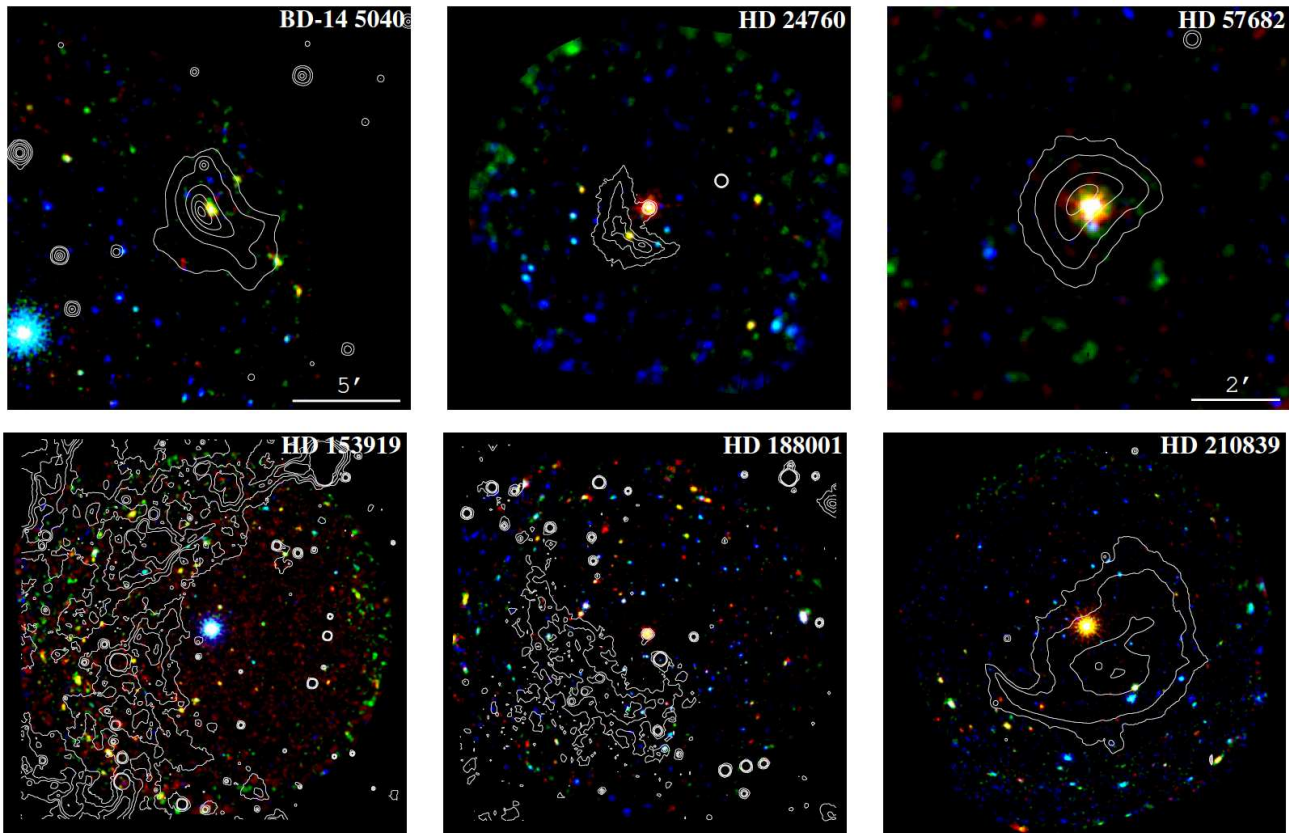


Figure 2. *XMM-Newton* EPIC (pn+MOS1+MOS2) exposure-corrected, background-subtracted X-ray images of the six bow shocks studied in this paper. Red, green, and blue correspond to the soft (0.3 - 1.0 keV), medium (1.0 - 2.0 keV), and hard (2.0 - 5.0 keV) bands, respectively. The progenitor stars are placed at the center of each panel. Contours show the *WISE* W4 22 μ m emission from the bow shock on each panel. North is up, east is to the left.

shows that our estimated observed fluxes are comparable to those reported by [Toalá et al. \(2016\)](#) for ζ Oph and BD+43°3654.

Our systematic search using a clean sample of runaway massive stars add to the list of bow shocks around runaway stars without non-thermal diffuse X-ray emission ([Terada et al. 2012](#); [Toalá et al. 2016](#)). Our present results encouraged us to question the previously claimed detection of non-thermal X-ray emission in the bow shock around AE Aur ([López-Santiago et al. 2012](#)). In Appendix A, we show that the detected emission is a point-like source unrelated to the bow shock around AE Aur.

It has become evident that current theoretical models overpredict the flux of the non-thermal diffuse X-ray emission in bow shocks around runaway. To start with, [del Valle & Romero \(2012\)](#) adopted a mass-loss rate a factor of ~ 5 greater than that reported by [Gvaramadze et al. \(2012\)](#), overestimating the density of high-energy particles. On the other hand, unlike the cases of supernova remnants which are known to emit considerably non-thermal X-ray emission (e.g., [Bamba et al. 2005](#)), the open morphologies of bow

shocks around runaway stars might reduce the injection efficiency of energy from thermal plasma to accelerate particles and produce non-thermal emission.

5. CONCLUSIONS

We have searched for non-thermal diffuse X-ray emission associated with bow shocks around runaway O-type stars. We used *XMM-Newton* observations of a sample of 6 well determined runaway stars and found no evidence of such emission.

We also revised the only claimed case of non-thermal diffuse X-ray emission detected from a bow shock, AE Aur. There is emission; however, its spatial distribution is consistent with being that of a point source. Moreover, this X-ray source is not spatially coincident with the bow shock. Thus, we conclude that this X-ray emission is not associated with the bow shock.

Thus far, there are 9 bow shocks around O stars that stand in defiance of the recent and growing body of theoretical predictions for non-thermal diffuse X-ray emissions from such structures. We conclude that, if this predicted non-thermal diffuse X-ray emission is present in bow shocks around runaway O stars, it is

below the detection limits of the current X-ray satellites.

The authors would like to thank the anonymous referee for valuable comments that improved our manuscript. This work was based on observations obtained with *XMM-Newton*, an ESA science mission with instruments and contributions directly funded by ESA Member States and NASA. This publication also makes use of data obtained with *WISE* and *Spitzer*. (*WISE*)

APPENDIX

A. AEAURIGAE

The absence of non-thermal diffuse X-ray emission towards the sample of six bow shocks presented in this paper, along with previously reported undetections (see Section 1), questions the nature and presence of the X-ray emission towards AE Aur reported by López-Santiago et al. (2012). To confirm previous results, we have analyzed the *XMM-Newton* observations

of AE Aur in a similar way as described for other sources studied here. We compare our X-ray images to *Spitzer* MIPS and IRAC images.

The left panel of Figure 3 shows the higher-resolution image of the *Spitzer* data as compared to the *WISE* W3 image (see figure 1 in López-Santiago et al. 2012). On the other hand, the right panel of Figure 3 presents a comparison of the *Spitzer* IRAC 8 μm and the medium and hard X-ray bands. This panel confirms that the blob of X-ray emission has a point-like shape with an angular separation of $35''$ from AE Aur, but also that this emission is not spatially coincident with the bow shock around AE Aur. The position of the blob of X-ray emission is shown in Fig. 3-right panel with a (white) solid line circular aperture. This X-ray blob is not one of the dense molecular globules detected in CO $\sim 25''$ from AE Aur (see globule #5 in figure 2 of Gratier et al. 2014). Thus, we can not confirm the previous claims on non-thermal emission associated with the bow shock around AE Aur.

REFERENCES

- Bamba, A., Yamazaki, R., Yoshida, T., Terasawa, T., & Koyama, K. 2005, *ApJ*, 621, 793
- Benaglia, P., Romero, G. E., Martí, J., Peri, C. S., & Araudo, A. T. 2010, *A&A*, 517, L10
- Blaauw, A. 1961, *BAN*, 15, 265
- Brown, A. G. A., Vallenari, A., et al. 2016, *A&A*, 595, A2
- del Valle, M. V., Romero, G. E., & Santos-Lima, R. 2015, *MNRAS*, 448, 207
- del Valle, M. V., & Romero, G. E. 2014, *A&A*, 563, A96
- del Valle, M. V., & Romero, G. E. 2012, *A&A*, 543, A56
- Gratier, P., Pety, J., Boissé, P., et al. 2014, *A&A*, 570, A71
- Gies, D. R., & Bolton, C. T. 1986, *ApJS*, 61, 419
- Gvaramadze, V. V., Langer, N., & Mackey, J. 2012, *MNRAS*, 427, L50
- Hoogerwerf, R., de Bruijne, J. H. J., & de Zeeuw, P. T. 2000, *ApJL*, 544, L133
- Kaper, L., van Loon, J. T., Augusteijn, T., et al. 1997, *ApJL*, 475, L37
- López-Santiago, J., Miceli, M., del Valle, M. V., et al. 2012, *ApJL*, 757, L6
- Maíz Apellániz, J., Barbá, R. H., Simón-Díaz, S., Negueruela, I., & Trigueros Páez, E. 2016, arXiv:1612.07923
- Pereira, V., López-Santiago, J., Miceli, M., Bonito, R., & de Castro, E. 2016, *A&A*, 588, A36
- Peri, C. S., Benaglia, P., & Isequilla, N. L. 2015, *A&A*, 578, A45
- Schulz, A., Haupt, M., Klepser, S., & S. Ohm for the H. E. S. S. Collaboration 2016, arXiv:1611.08197
- Schulz, A., Ackermann, M., Buehler, R., Mayer, M., & Klepser, S. 2014, *A&A*, 565, A95
- Snowden, S. L., & Kuntz, K. D. 2011, *Bulletin of the American Astronomical Society*, 43, 344.17
- Terada, Y., Tashiro, M. S., Bamba, A., et al. 2012, *PASJ*, 64, 138
- Toalá, J. A., Oskinova, L. M., González-Galán, A., et al. 2016, *ApJ*, 821, 79

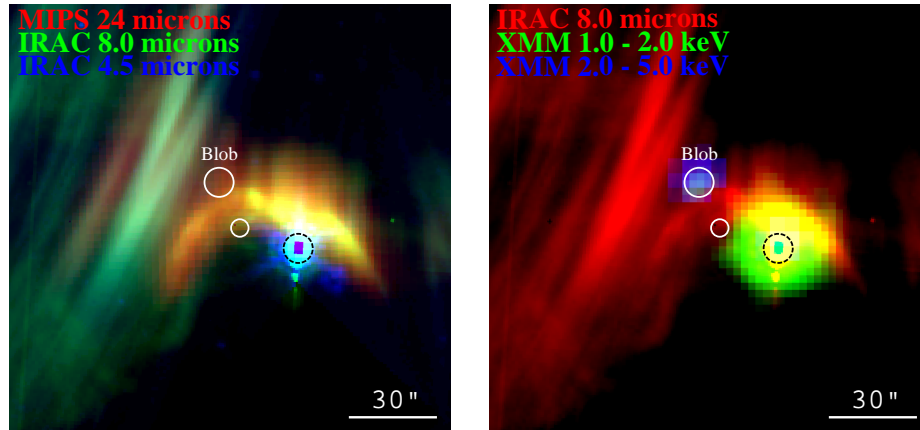


Figure 3. Composite colour images of the bow shock around AE Aurigae. North is up, and East is right. Left: Red, green, and blue correspond to *Spitzer* MIPS 24 μm , IRAC 8 μm , and IRAC 4.5 μm , respectively. Right: Red corresponds to the *Spitzer* MIPS 8 μm observation whilst green and blue correspond to the medium (1.0 - 2.0 keV) and hard (2.0 - 5.0 keV) bands, respectively. The position of AE Aur is shown with a (black) dashed-line circular aperture and the position of the X-ray blob is shown with a (white) solid-line circular aperture whilst the position of the CO globule #5 as reported by [Gratier et al. \(2014\)](#) is shown by the smaller circular aperture.